The Relationship Between Dust Lanes and Active Galactic Nuclei

MacKenzie Dean, University of Colorado, Boulder

Advisor: Dr. Michael Koss, Eureka Research

Abstract

We investigate the influence of optically obscuring dust lanes on numerous characteristics of active galactic nuclei (AGN) in the redshift range $0.001 < z < 0.1$ to include Seyfert type classifications, column density, bolometric luminosity and Eddington ratios. Building our sample of 336 AGN from the 70-month *Swift*/BAT and using optical images of each object taken by the Hubble Space Telescope, we use visual determinations to catalogue each sample object in accordance with the existence and extent of identifiable dust lane features across nuclear and galactic scales. Comparing these characteristics together, we analyze the role of dust in AGN and find that the existence of dust lanes in and/or around AGN do not significantly influence AGN growth rate. However, to make a definitive conclusion regarding the full scope of the role that dust plays in regards to AGN, there is a requirement for analysis of large samples that cover a broader region of redshift values as well as detection and imaging instruments with higher sensitivity to objects that lie closer to the extremes of AGN characteristic limits.

1 Introduction

Observational evidence suggests that most major galaxies host supermassive black holes (SMBH, $10^{6-9.5}M_{\odot}$) at their centers, some of which are in a phase of active material accretion. Supermassive black holes of this type, known as active galactic nuclei (AGN), are highly energetic objects that radiate in numerous spectral ranges as material inflow causes the object to increase in size but the origin of the inflowing material and the scope of influence it has on the growth rate of AGN is not currently well understood. Early studies and observations suggest that a source of this inflowing material could be what we have identified as being optically obscuring dust, or dust lanes which are commonly found in and around galactic nuclei, but the large-scale samples that are necessary for a broader, stronger understanding of the relationship between dust and AGN growth have yet to be created or examined.

Dust lanes are most easily identifiable in the optical radiation band (Ramos Almeida & Ricci 2017), due to the absorption of visible light that is emitted from the AGN. The Hubble Space Telescope (HST) is capable of imaging these nearby AGN in the optical spectral range at 10-20 times greater spatial resolution than ground-based observatories and this resolution achievement is necessary for the visual probing of galactic nuclei and therefore, the identification of any present dust lanes (Malkan et al. 1998). Visual identification of dust lanes then informs our classifications of the observed AGN, which is key to assess any relationships between obscuring dust and AGN.

Morphology heavily relies on the existence of dust in and around all galaxies, to include AGN, which offers an opportunity to identify relationships between morphology and AGN growth rate. Previous studies suggest that the morphology of a galaxy, and therefore the dust within, aids in the process of AGN growth such that the existent dust is a source of material being acreted by the central supermassive black hole (Maiolino et al. 1999). Concurrently, studies have also suggested

that the central engine of a galaxy influences the morphology of the galaxy as a whole (Macchetto 1999) further supporting the possibility of an intricate relationship between morphological dust and AGN growth rates. An important consideration to make when investigating the relationships between the existence of dust lanes and galaxy morphology, to then be applied to AGN growth rate, is the orientation of the observed galaxy with respect to the observer's line of sight as the viewing angle of the object heavily influences the appropriate identification of dust features and the scale in which they are found (González-Martín, O. et al. 2013). The broader implications of orientation on our current understanding of AGN has been further explored within the bounds of the proposed unified model of AGN (Bianchi et al. 2012), in which our following investigation hopes to prove useful.

Additionally, X-ray obscuration of AGN is commonly attributed to the varying levels of column density, N_H, or obscuring material within the central parsecs of the observed AGN (Guainazzi et al. 2005), (Malizia, A. et al. 2020). High column density ($N_H \geq \sigma_t^{-1} \simeq 1.6 \times 10^{24} cm^{-2}$) is considered as being "Compton-thick" while low column density ($N_H \geq \sigma_t^{-1}$) is classified as "Compton-thin". The existence of this material and subsequent obscuration is widely considered to correlate with Seyfert classifications of galaxies such that Seyfert 2 galaxies are commonly observed to be obscured in the x-ray bandwidth by high column density material and Seyfert 1 galaxies are not (Guainazzi et al. 2001). AGN obscuration and emitted radiation has also been loosely connected to galactic morphology, where galaxies with a prominent disk component (Hubble classifications Sa – Sc) correlate strongly with x-ray emission and therefore obscuration so long as obscuring material is present near the galactic nucleus (Griffith & Stern 2010). Previous analysis of dust in the central parsecs of unobscured AGN has been conducted (Prieto et al. 2021), and reported results state that dust is ubiquitous in the central region of type 2 AGN, or optically obscured AGN without a broad line region (BLR) and that this observation is expected to further apply to type 1 AGN that do exhibit a BLR. Current limitations of this survey and others are the small sample sizes, where the above analyzes nine nearby AGN.

Finally, bolometric luminosity (L_B), refers to the total luminosity of the accretion disk of the AGN and therefore strongly correlates to the rate of accretion of the active nucleus and suggests a relationship with the growth rate of the AGN (Suh et al. 2015). In addition to bolometric luminosity, Eddington luminosity of AGN can determine the maximum radiation pressure such that material falls inwards towards the black hole rather than being forced outwards. Together, available data for the bolometric luminosity and Eddington luminosity of each object can be combined as an Eddington ratio ($\lambda = L_B/L_{Edd}$), which yields an estimate of the nuclear growth rate that we can then analyze against previously determined dust features.

Throughout this paper, we use comparative analysis to develop a better understanding of the influence of galactic dust on AGN growth rate. In section 2, we build our sample of 336 nearby AGN ($z < 0.1$) and discuss the methodology for visual identification of dust features and subsequent classifications of the sample as a whole. In section 3, we report the results of our comparative analysis between the sample's determined dust features and redshifts against several other properties of each AGN, including, Seyfert type, X-ray obscuration (column density, N_H), bolometric luminosity (L_B) and Eddington ratios (λ). Finally in section 4, we discuss the meanings and implications of our findings, address their contributions to our current understanding of the role dust plays on galactic scales and consider future applications of the work presented.

2 Data and Methods

2.1 Our Sample

Our sample comes from a parent sample of AGN that were detected in the 70-month Swift-Burst Alert Telescope (BAT) all sky survey (Ricci et al. 2017). The first selection criteria for our sample was based on electromagnetic emission, such that objects selected emitted in the hard X-ray which allows for the detection of highly obscured AGN (Koss et al. 2022). Of the parent sample, 858 AGN were identified as emitting in the hard X-ray. From here, objects were classified as beamed and unbeamed, and our sample downsized to 700 unbeamed objects. Finally, we determined our remaining sample objects by their calculated redshift. Redshift was chosen as selection criteria due to the resolution capabilities required to probe the central parsecs of each object for optimal identification of dust lanes. With this resolution limitation, we required that each object must be at redshift $z < 0.1$ because the resolution of the Hubble Space Telescope is 0.1" at this distance, meaning it is still sensitive up to 200kpc. After all cuts were made, we had our final sample of 342 nearby AGN.

Once our sample was constructed, we obtained reduced HST data for each object from the Barbara A. Mikulski Archive for Space Telescopes (MAST) Database. Using the online MAST archives from the Hubble mission, each object name was searched for as a science image with parameters of exposure time $> 10s$ and used filters to include F606W and F814W. A single data set for each sample object that was available was then downloaded as a drizzled image. Drizzled images were preferred due to the processing methods used to reconstruct the undersampled images and recombine them as a single scientific data set. There were 6 selected objects in our sample that had either not been imaged with HST in an optical bandwidth or had unusable data, which brought out usable sample size down to 336 objects.

About 80 percent of the images that were obtained for our sample came from an ACS imaging survey of nearby active galaxies lead by Aaron Barth, HST Proposal 15444. The remaining objects in our sample were imaged through various other HST proposals but all objects were imaged by one of three HST instruments: the Advanced Camera for Surveys (ACS), the Wide Field Camera 3 (WFC3) or the Wide Field and Planetary Camera 2 (WFPC2).

2.2 Sample Demographics

Demographics of our sample of 336 AGN, not including classifications based on the visual identification of dust, are outlined in accordance with the characteristics that were used for comparative analysis throughout the paper, to include redshift (z), Seyfert type, column density (N_H), bolometric luminosity and Eddington ratios (Table 1).

Table 1. Sample AGN Demographics

Object	Morphology	Redshift (z)	Seyfert Type	N_H ($10^x cm^{-2}$)	Bol. Lum. ($\frac{erg}{s}$)	Edd. Ratio (λ)
Mrk 78	Elliptical	0.0373091	Sy2	23.01	6.59E+43	0.00538156
3C403	Elliptical	0.05839908	Sy2	20	1.21E+44	0.02557645
NGC 5194	Spiral/Merger	0.001	Sy2	N/A	1.08E+40	0.000316742
NGC 3998	Lenticular	0.00357417	Sy1.9	20.81	1.71E+41	2.36E-05
NGC 3079	Uncertain	0.00350451	Sy2	26	3.36E+41	0.11127085
NGC 4395	Spiral	0.00110586	Sy1	21.08	3.20E+40	0.011256885

Note. — Table 1. Morphology classifications of each sample object were obtained from GalaxyZoo (https://www.zooniverse.org/projects/zookeeper/galaxy-zoo/) and all other demogrphics were reported in the 70-month Swift-Burst Alert Telescope (BAT) all sky survey (Koss et al. 2022).

Morphology of our sample includes spiral, elliptical, lenticular, mergers and/or disturbed galaxies and a supplementary category of uncertain morphology, which refers to galaxies that are at an orientation with respect to our line of sight that prohibits a definitive assignment of the previously established classifications. These classifications were determined and assigned based on previous classifications from GalaxyZoo and supplemented by visual assessment that was conducted simultaneously to the process of visually identifying dust features in each sample object.

As shown (Figure 1), our sample was broken down by the existence of dust features with respect to the scales of observed dust features and the morphology of each object in the sample. In broader classification, about 44 percent of the objects that were classified as having identifiable dust features were categorized as spiral galaxies, 17 percent were elliptical galaxies, another 17 percent were merging systems or severely disturbed objects, 12 percent were categorized as having an uncertain morphology and the final 10 percent were identified as lenticular galaxies.

Redshift is included in our demographics due to it's contribution towards the possible identification of dust as well as influence it has on AGN characteristic identification such as bolometric luminosity and Eddington ratios. As the universe is expands, the light that is traveling through it is being stretched and the observed result of this expansion is known as cosmological redshift. This means that the light that we observed of each object in their respective Hubble optical image was

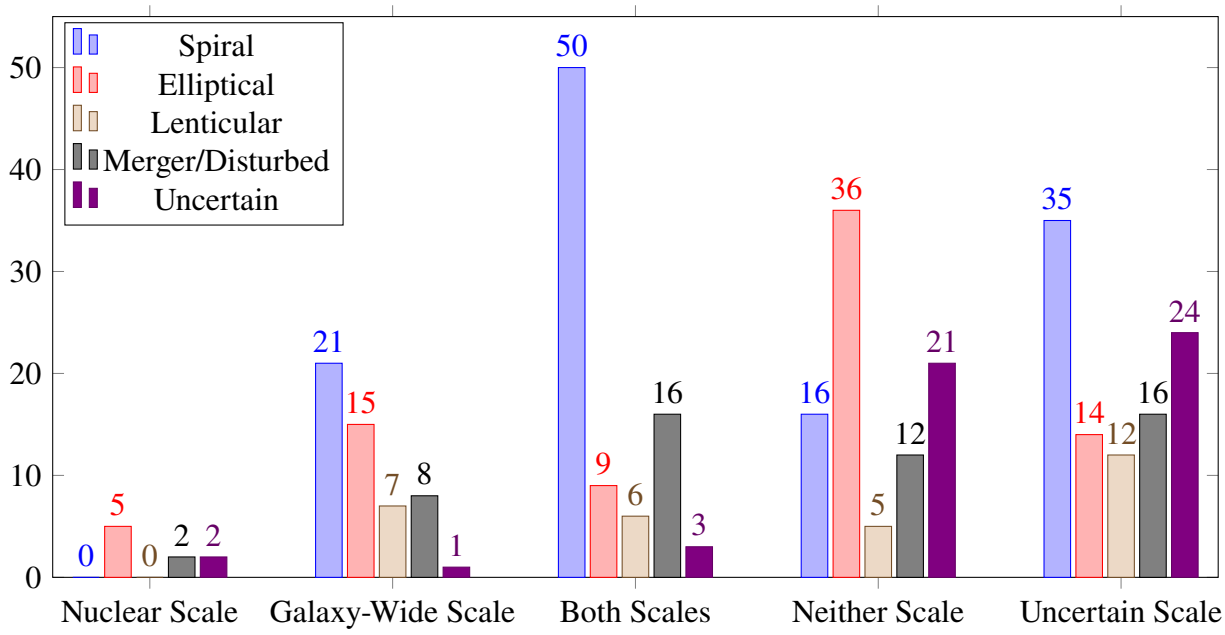

Fig. 1.—: Observed scales of dust lane features by galaxy morphology. Uncertain categories refer to the objects within the sample that are at an orientation with respect to our line of sight that inhibits the definitive classification of dust lane locations and/or galaxy morphology.

emitted at a time when all of the galaxies in the universe were 10 percent closer than they are today. In physical distance, this upper limit corresponds to a maximum distance of 1.3 billion light years away from us.

Objects were categorized first by the existence and location of identifiable dust features, or the lack thereof, and then classified by their calculated redshift (Figure 2). As shown, objects that were classified as having visible dust features follow the trend that more of these objects were found at lower redshifts than higher. This is to be expected as the resolution of each image decreases as redshift increases, meaning that this result could prove to be based in bias by imaging capabilities. This bias could further be exasperated by the results of the objects that have no dust features, as there does not seem to be as extreme of a decreasing in the lack of identifiable dust lanes as redshift increases.

2.3 Dust Features of Our Sample

Once obtained, object images were visually inspected for dust feature classification using SAOImageDS9, which allowed for the manual adjustment of pixel values, zoom and stretch scales, all of which were necessary for the visual identification of nuclear and galaxy-wide dust lanes. Once each image is loaded, a log scale was applied to redefine the color distribution of the pixels in aim to resolve issues with an overly bright nuclear region of the galaxy. This allows for a smaller contrast ratio surrounding the AGN to identify extinction, or dust lanes along the line of sight, near the galactic nucleus or across the entire galaxy depending on the sample.

Classification prompts, (Table 2) were used in this process to uniformly assess each AGN individually based on the existence of dust features, locations of such features if they exist and commentary

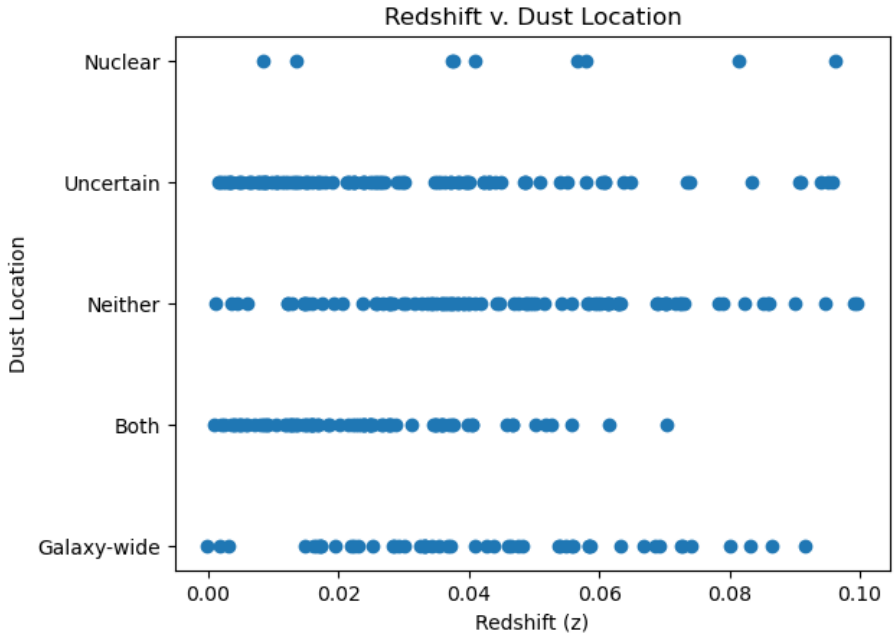

Fig. 2.—: Redshift and Dust. This graph compares the calculated redshift of each object and the locations in which dust lanes were identified in each object.

on any uncertainties throughout the inspection process. The basis of common uncertainties included the orientation of the galaxy from our line of sight, which limited the visual of the AGN, specifically if the galaxy appeared edge-on in the obtained image and any resolution restrictions that could not be worked around such as the AGN being luminous enough to be recorded as a point source in the image, rendering the image contrast manipulation useless for identification of dust in the inner parsecs of the nucleus. Several rounds of visual identification and dust feature classifications were conducted.

Out of our sample of 336 AGN, 246 objects were classified as exhibiting dust features on some scale including nuclear, galaxy-wide or both and the other 90 objects exhibit no distinct dust (Figure 3a). An important fourth categorization of our sample objects are those that exhibit dust lanes on some scale, but due to their orientation with respect to our line of sight, we are unable to conclusively say whether or not the observed dust lanes are around the galactic nucleus. There are 101 objects within our sample that fall into this category (Figure 4e).

More explicit classifications (Figure 3b) show that 9 of the 246 objects that exhibit dust on some scale exhibit only nuclear dust lanes, 52 objects exhibit only galaxy-wide dust lanes and 84 objects exhibit dust lanes across both scales (Figure 4a-c). AGN that fall into the category of exhibiting dust features on both scales are not ones that are observed at an obstructing orientation, meaning that the visual identification of dust in these cases are certain.

Majority of the 90 objects that were identified as having no dust features were done so confidently as images that showed the AGN and greater galaxy were available (Figure 4d) but few objects were noted as imaging similarly to a point-like object, inhibiting the identification of dust within the galaxy or around the nucleus. In this case, the AGN were classified as having no nuclear dust

Table 2. Sample Dust Classifications

Object Name	Dust Features	Orientation	Location	Uncertainties	Notes
Mrk 78	Yes	No	Nuclear	No	None
3C403	Yes	No	Galaxy-wide	No	None
NGC 5194	Yes	No	Both	No	None
NGC 3998	No	No	Neither	No	Point-like Nucleus
NGC 3079	Yes	Yes	Galaxy-wide	Yes	Orientation
NGC 4395	No	No	Neither	Yes	Point-like Image

Note. — Table 2. Dust classifications were assigned manually to every sample object during the visible inspection of each HST image through SAOImageDS9. The classifications outlined above were refined through several rounds of inspection of each image to support consistent classification.

features so long as no other dust features on other scales were visually identifiable (Figure 4f).

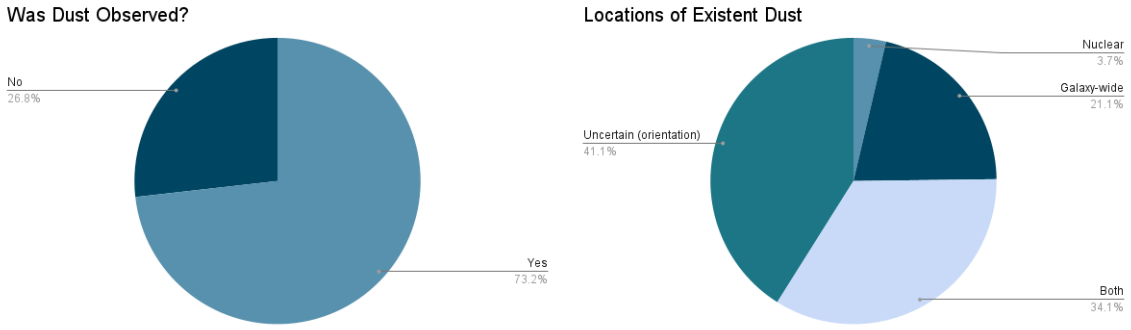

(a) (b)

Fig. 3.—: (a) Percentages of sample that show any dust or not. (b) Scales of dust that was observed

3 Results

3.1 Seyfert Types

Our sample is originally broken down into six different Seyfert classifications: Sy1, Sy1.2, Sy1.5, Sy1.8, Sy1.9 and Sy2 (Figure 5) but for simplicity of analysis, we regroup the sample into two categories: Sy1 (include: Sy1, Sy1.2, Sy1.5, and Sy1.8) and Sy2 (include: Sy1.9 and Sy2) which correlate the nuclear region's spectra of the applicable object to having broad emission lines or narrow emission lines respectively. The width of these emission lines correspond to the velocities of expanding hot gas within the central region of the sample object such that broad emission lines indicate higher velocities and narrow emission lines indicate more modest velocities. Furthermore, Sy1 galaxies are considered to be have more direct line of sight to their nuclear region whereas Sy2

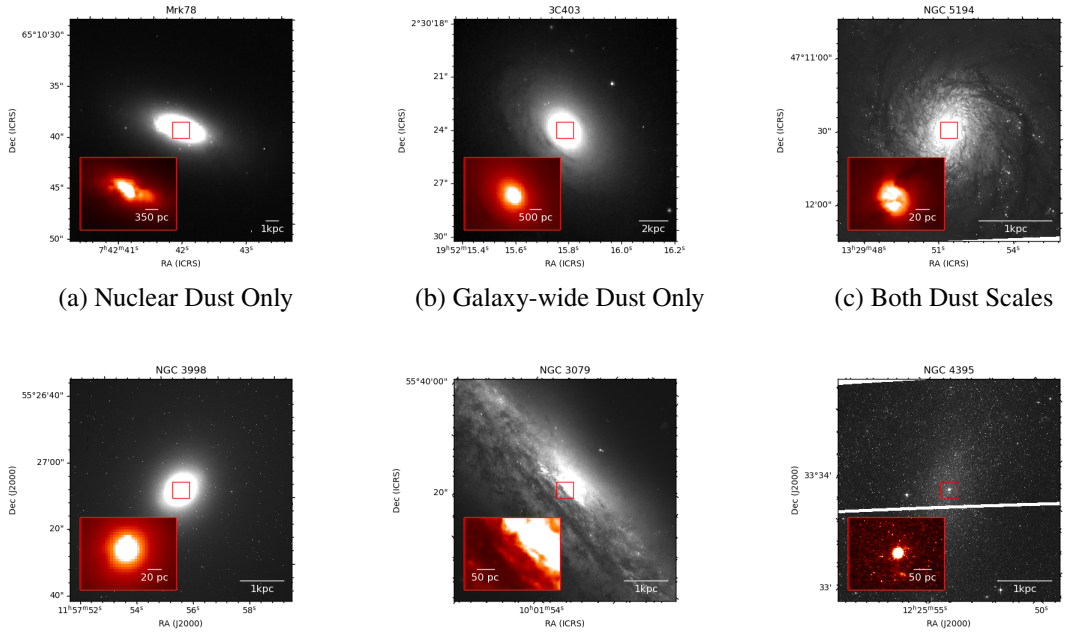

(a) Nuclear Dust Only (b) Galaxy-wide Dust Only (c) Both Dust Scales

(d) Neither Dust Scale (e) Uncertain by Orientation (f) Point-like Objects

Fig. 4.—: Examples of dust lane scale classifications. From top to bottom, left to right: (a) Mrk78: Nuclear dust lanes only, (b) 3C403: Galaxy-wide dust lanes only, (c) NGC 5194: Dust lanes across both nuclear and galaxy-wide scales, (d) NGC 3998: no dust lanes, (e) NGC 3079: uncertain dust lane scales due to orientation, (f) NGC 4395: point-like source (no dust lanes).

nuclei are more obscured and only the colder, outer regions of the nucleus are observable.

Analysis of Seyfert classification with respect to the location of dust features that were observed or not in each object of our sample (Figure 6a) are as expected. As shown, there are more Sy1 AGN in our sample that exhibit no dust features as compared to the objects that are classified as being Sy2 objects and with that, there are more Sy2 objects that exhibit dust lane features on some scale than there are Sy1 objects. When it comes to objects that do exhibit dust lane features in our sample, Sy1 objects are more likely to exhibit galaxy-wide dust features which aligns with Sy1 objects having a characteristically more visible nuclear region than Sy2 objects. Additionally, Sy2 objects are more commonly observed as having dust lanes in or around the nuclear region, again aligning with the higher obscuration levels of nuclear regions in these objects. Finally, the sample objects that are classified as having dust with uncertain locations are prominently categorized as Sy2, which is an expected result as the uncertain category is mostly comprised of objects that are at an orientation with respect to our line of sight that allows the positive identification of dust but prohibits an assignment of the location of the dust, further obscuring the nuclear region of the applicable objects. After analysis, we comfortably conclude that there is no remarkable relationship between dust features and Seyfert classifications.

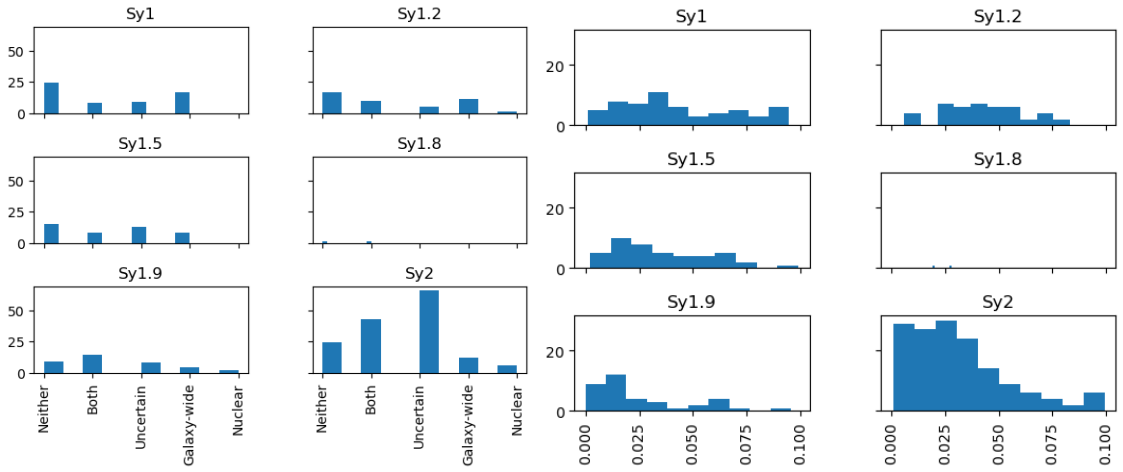

(a) Seyfert Type and Dust Location (b) Seyfert Type and Redshift

Fig. 5.—: Seyfert Types. Graph (a) shows the distribution of object Seyfert classifications against the locations of any identified dust features and graph (b) shows the distribution of object Seyfert classifications against calculated redshift values (z) of each object.

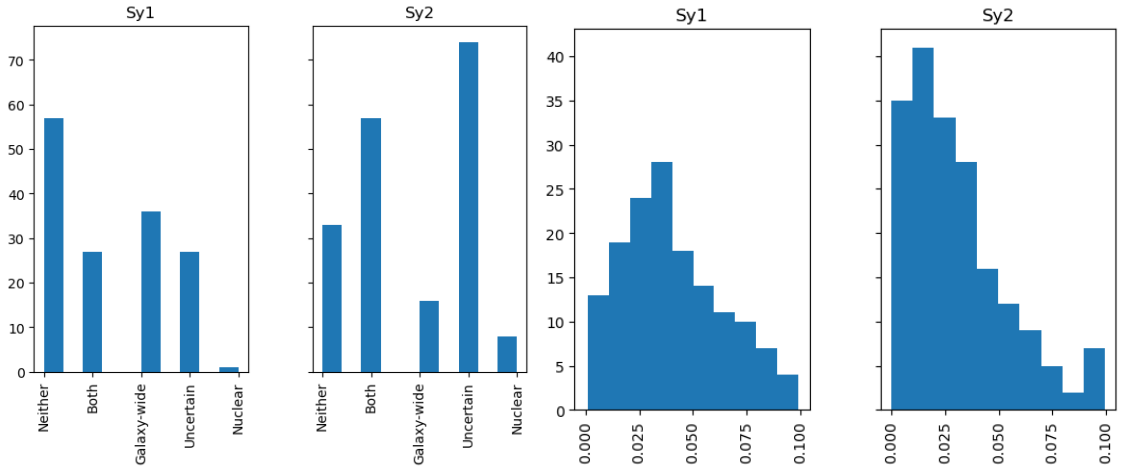

(a) Simple Seyfert Type and Dust Location (b) Simple Seyfert Type and Redshift

Fig. 6.—: Simple Seyfert Types. Graph (a) shows the simple distribution of object Seyfert classifications against the locations of any identified dust features and graph (b) shows the simple distribution of object Seyfert classifications against calculated redshift values (z) of each object.

3.2 Column Density

Column density, N_H, refers to the number of molecules/cm^2 along the line of sight toward the object being observed. For our sample, measured column density spans seven orders of magnitude, $10^{20-26} cm^{-2}$ and the classification of low column density refers to objects with measured $N_H < 10^{24} cm^{-2}$ and high column density indicates $N_H > 10^{24} cm^{-2}$.

Graphical results (Figure 7a) show that majority of our sample exhibit low column density

measurements, but do not indicate a strong relationship between the existence of dust lane features and column density as varying column densities are observed across all dust classifications. It is important to note that objects exhibiting only galaxy-wide dust features were not observed to have particularly high column densities, Additionally, contrary to expectations, sample objects that exhibited no dust lane features appear to span the entire range of column densities. Finally, there is a significant gap in column density range $10^{25-26} cm^{-2}$ for objects that exhibit dust either somewhere (uncertain), nowhere or everywhere (both). Seeing that column density does not present a graphical correlation with dust features, we conclude that dust does not have a significant relationship to this AGN characteristic.

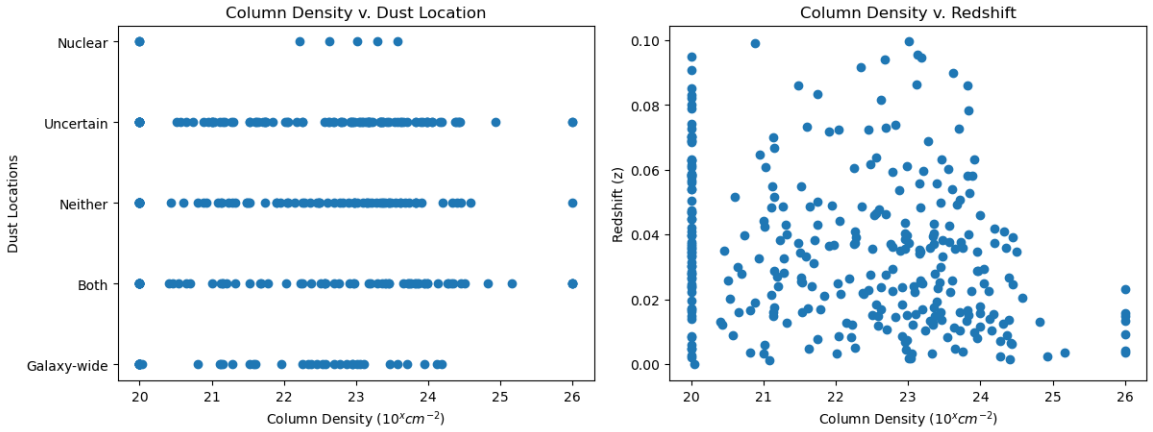

(a) Column Density and Dust Location

(b) Column Density and Redshift

Fig. 7.—: Column Density. Graph (a) shows the distribution of object column density measurements against the locations of identified dust features in each object and graph (b) shows the distribution of object column density measurements against calculated redshift values (z).

3.3 Bolometric Luminosity

Bolometric luminosity is used here to assess the luminosity of the AGN in totality and is loosely proportional to accretion rates of the AGN and therefore may relate to the growth rate of AGN. Objects in our sample span the range $L_B \sim 10^{39-45} \frac{erg}{s}$.

Majority of sample objects measure $L_B > 10^{42} \frac{erg}{s}$ and this trend is present in all dust location scales including objects that exhibit no dust features (Figure 8a). This is most likely due to the sensitivity of the instrumentation used to detect AGN throughout the *Swift*/BAT survey from which our sample originated. An important qualitative observation is that objects that exhibit only nuclear dust features measure a higher bolometric luminosity average than other dust feature scales although this could be due to the sample size in which only nine objects exhibit nuclear dust lanes exclusively. Additionally, only five sample objects measure $L_B < 10^{41}$ which further supports the assumption that instrumentation sensitivity is an important factor of our available data and the analysis we are able to conduct with it. Since luminosity trends are seemingly uniform across all dust feature scales, we conclude that there is minimal to no definitive relationship between dust lanes and bolometric luminosity.

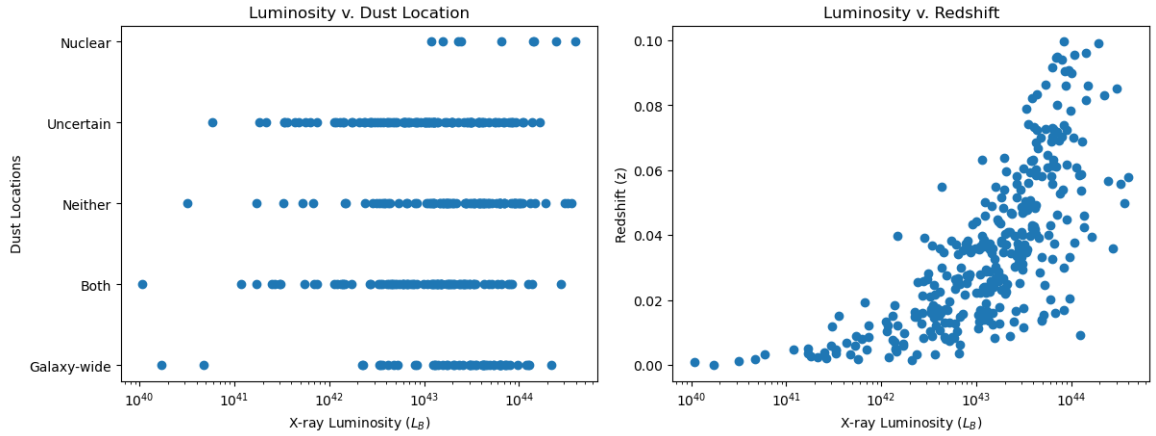

(a) Bolometric luminosity and Dust Location

(b) Bolometric luminosity and Redshift

Fig. 8.—: Bolometric luminosity. Graph (a) shows the distribution of object bolometric luminosity measurements against where dust lanes were identified and graph (b) shows the distribution of object bolometric luminosity measurements against the calculated redshift values (z).

3.4 Eddington Ratio

Bolometric luminosty and Eddington limits can be combined to define the Eddington ratio (λ) of an AGN object such that $\lambda = \frac{L_B}{L_{Edd}}$. This term can then be used to determine changes in accretion rates of AGN over cosmic time, but for our purposes, we use it to assess any correlation between the existence of dust in the nuclear region of AGN or the host galaxy as a whole. Our sample spans a Eddington ration range $\lambda \sim 10^{0-3}$.

Our sample does not suggest a notable relationship between dust lanes and Eddington ratios, as seen by a uniform distribution of higher Eddington ratios in every dust lane scale classification (Figure 9a). Majority of sample objects have measured $\lambda > 10^1$, including objects that exhibit no dust features which indicates that the galactic dust in and around AGN may not be significant contributors to AGN accretion rates and by extension, AGN growth rates. Interestingly, there are very few objects that measure $\lambda \sim 10^0$ but again these objects are not uniform in the dust features they exhibit further inhibiting the identification of a remarkable relationship between dust and Eddington ratios.

4 Discussion

We discuss the possible influence of varying redshift (z) values and the implications this may have on our observations, measurements and results for each object with respect to Seyfert type, column density, bolometric luminosity and Eddington ratios. To explore these effects, we analyze our sample in each of these demographic categories against object redshift values (z). It is important to note that the range of redshift values of our sample is not large enough to be applicable to evolution of our sample objects over cosmic time, therfore this consequence of cosmological redshift goes unaddressed in our discussion.

As shown above (Figure 6b), our sample has a higher concentration of Sy2 AGN, making up 188

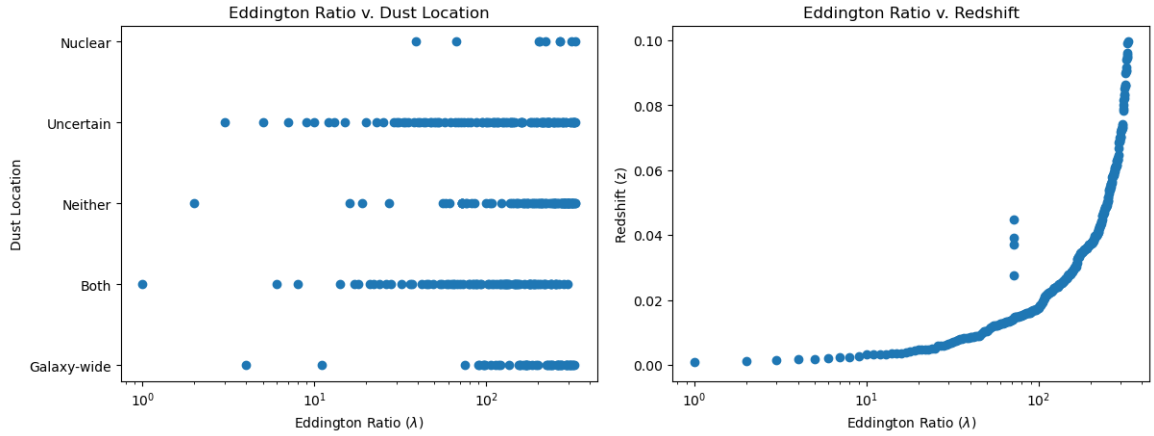

(a) Eddington Ratio and Dust Location

(b) Eddington Ratio and Redshift

Fig. 9.—: Eddington Ratio. Graph (a) shows the distribution of object Eddington ratio calculations against where dust lanes were identified and graph (b) shows the distribution of object Eddington ratio calculations against the calculated redshift values (z).

out of 336 objects, as compared to Sy1 AGN which totals the remaining 148 objects. For sample objects that are classified as Sy1, counts with respect to redshift appear parallel to our sample as a whole, where majority of observed objects fall between $0.025 < z < 0.075$ which suggests that our observations are not due to unaddressed bias. Additionally, in contrast to objects that are categorized as Sy2, there are more Sy1 galaxies found at higher redshifts, $z > 0.05$, which agrees with observational capabilities such that unobscured nuclear regions allow for easier detection at farther distances. Our observations in this regard also agree in the case of Sy2 objects, such that more obscured nuclei are found at lower redshift, $z < 0.05$. This implies that while our sample may not have an equal count of Sy1/Sy2 objects in each redshift benchmark, there is no obvious reason to suspect that there are not equal distributions of these objects across the universe.

Graphical results of the distribution of object column density against calculated redshift values (z) (Figure 7b) indicate that objects exhibiting low column density were detected across all redshift benchmarks. This is an expected result as column density directly correlates to emission absorption around the nuclear regions of AGN and lower column density inhibits higher absorption levels. In contrast, objects with high column densities were not detected beyond $z = 0.03$. This result is also likely due to the absorption properties of the obscuring material noted by $N_H > 10^{24} cm^{-2}$ and supports the understanding that objects at farther distances are more difficult to detect as apparent brightness is inversely proportional to distance squared. Furthermore, there is a negative linear relationship between the limit of detected object column density and redshift such that objects with $N_H > 10^{23} cm^{-2}$ cease to be detected at $z = 0.1$ and as column density increases, detected objects are found at lower redshifts. Again, this result may be caused by technological limitations as more obscured object become more difficult to detect at far distances.

Measured luminosity of celestial objects is not dependent on the distance between the observer and the observed and our sample supports this understanding, as seen in Figure 8b, where a logarithmic fit is apparent. In this comparison, we see that objects across the entire luminosity

range are found at lower redshifts, but we do not see objects of lower luminosity at high redshifts. This trend supports the hypothesis that instrumentation sensitivity influenced our sample rather than possibility that low luminosity AGN do not exist at larger distances away from us. Similar results when analyzing Eddington ratios with respect to redshift are present and expected due to Eddington ratios being a function of multiple luminosity values. There is a stronger logarithmic fit in the graphical representation of Eddington ratios (Figure 9b), but there are four outlying objects that beg further investigation at another time.

While our sample is one of the largest used for comparative analysis of AGN, 336 objects is seemingly too few to understand the full scope of influence that galactic dust has on supermassive black holes and their host galaxies. In order to expand that understanding, we would require more objects at a larger range of redshift parameters to get a more comprehensive view of the reach of galactic dust lanes but for now, we have a better grasp on 336 nearby AGN and several of their characteristics, to include morphology, redshift, Seyfert classification, column density, bolometric luminosity, Eddington ratios and for the first time, dust lane features. This information proves useful in more specialized AGN research, specifically regarding small AGN samples and further investigation into the relationship dust has to the universe and how it's role may change over cosmic time.

5 Summary

We present an investigation into several proposed relationships that dust lane features could maintain with AGN, to include Seyfert type classifications, column density, bolometric luminosity and Eddington ratios through extensive comparative analysis of a large-scale AGN sample. Using previously determined values of object redshift and new visual classifications of dust features for each sample object, we expand on our current understanding of the role that dust plays on galactic scales. Our sample consists of 336 nearby AGN, such that $z < 0.1$, and spans a column density range $N_H \sim 10^{20-26} cm^{-2}$, bolometric luminosity range $L_B \sim 10^{39-45} ergs^{-1}$ and Eddington ratio range $\lambda \sim 10^{0-3}$ with logarithmic scaling.

Based on the comparative analysis conducted, we find that optically obscuring dust lanes are not significantly influential in the case of Seyfert type classifications, column density measurements, object bolometric luminosity or calculated Eddington ratios. Where there could have been an expected variance between objects with identifiable dust lanes and without, there were uniform distributions across the board, indicating that dust lanes do not act alone in the influence of AGN growth rate. However, to expand our understanding of the entire role that dust plays on galactic scales, it is required that larger sample sizes be analyzed, which extends to the needs for more sensitive instrumentation for the purpose of object identification and imaging.

We gratefully acknowledge the National Science Foundation's support of the Maria Mitchell Observatory's REU program through grant AST-2149985 as well as the support from the Maria Mitchell Association of Nantucket, Massachusetts. This research has made use of the MAST Archival database, operated at STScI, Baltimore, Maryland. This report makes use of HST Proposal 15444, an imaging survey of nearby AGN conducted by Aaron Barth.

References

Bianchi S., Maiolino R., Risaliti G., 2012, Advances in Astronomy, 2012, 1

González-Martín, O. et al., 2013, A&A, 553, A35

Griffith R. L., Stern D., 2010, AJ, 140, 533

Guainazzi M., Fiore F., Matt G., Perola G., 2001, Monthly Notices of the Royal Astronomical Society, 327, 323

Guainazzi M., Matt G., Perola G. C., 2005, A&A, 444, 119

Koss M. J., et al., 2022, The Astrophysical Journal Supplement Series, 261, 2

Macchetto F. D., 1999, Supermassive Black Holes and Galaxy Morphology (arXiv:astro-ph/9910089)

Maiolino R., Risaliti G., Salvati M., 1999, A&A, 341, L35

Malizia, A. Bassani, L. Stephen, J. B. Bazzano, A. Ubertini, P. 2020, A&A, 639, A5

Malkan M. A., Gorjian V., Tam R., 1998, ApJS, 117, 25

Prieto M. A., Nadolny J., Fernández-Ontiveros J. A., Mezcua M., 2021, MNRAS, 506, 562

Ramos Almeida C., Ricci C., 2017, Nature Astronomy, 1, 679

Ricci C., et al., 2017, ApJS, 233, 17

Suh H., Hasinger G., Steinhardt C., Silverman J. D., Schramm M., 2015, The Astrophysical Journal, 815, 129